Optical Engineering

OpticalEngineering.SPIEDigitalLibrary.org

Common-path all-fiber optical coherence tomography probe based on high-index elliptical epoxy-lensed fiber

Soohyun Lee
Changho Lee
Ruben Verkade
Gyeong Woo Cheon
Jin U. Kang

SPIE.

Soohyun Lee, Changho Lee, Ruben Verkade, Gyeong Woo Cheon, Jin U. Kang, "Common-path all-fiber optical coherence tomography probe based on high-index elliptical epoxy-lensed fiber," *Opt. Eng.* **58**(2), 026116 (2019), doi: 10.1117/1.OE.58.2.026116.

Common-path all-fiber optical coherence tomography probe based on high-index elliptical epoxy-lensed fiber

Soohyun Lee,[a,*] Changho Lee,[b] Ruben Verkade,[c] Gyeong Woo Cheon,[a,†] and Jin U. Kang[a]
[a]Johns Hopkins University, Department of Electrical and Computer Engineering, Baltimore, Maryland, United States
[b]Chonnam National University Medical School and Hwasun Hospital, Department of Nuclear Medicine, Hwasun, Republic of Korea
[c]Eindhoven University of Technology, Department of Mechanical Engineering, Eindhoven, The Netherlands

Abstract. We propose and demonstrate high-index elliptical epoxy-lensed fiber probes designed specifically for endoscopic common-path (CP) swept-source optical coherence tomography (OCT) imaging inside wet tissues. The high-index epoxy lens uses a beam expansion region of a few hundred microns, which is capped with a spherical surface mounted at the end of an optical fiber. The probe is designed to operate inside wet tissues and shows improved performance over a long imaging depth, compared to bare or simple half-ball-lensed fiber probes. It allows optimal CP-OCT imaging in wet tissues by providing a stable reference power level and optimal beam waist for a long imaging depth. We have fabricated an array of these probes and one with a beam expansion region length of 288 μm and with a lens surface radius of 61 μm exhibiting 25-dB signal-to-noise ratio improvement compared to a bare fiber probe at 1.5-mm distance in water. The proposed probe is tested using a phantom sample comprising several layers of tape in water. The OCT images show that the probe is capable of high-resolution imaging over a distance of 1.5 mm. [DOI: 10.1117/1.OE.58.2.026116]

Keywords: optical coherence tomography; lenses; fiber optic application; imaging system.

Paper 181721L received Dec. 9, 2018; accepted for publication Feb. 11, 2019; published online Feb. 28, 2019.

1 Introduction

Compact all-fiber optical coherence tomography (OCT) probes allow insertion into small and tight areas of the body, enabling catheter-based endoscopic imaging. There have been many studies using OCT endoscopic systems for clinical applications, including vascular, digestive, respirator, and reproductive systems.[1] Fiber-based endoscopic OCT probes have been developed for ophthalmic surgery and advanced microsurgical tools.[2–8] An example includes hand-held automatic OCT-distal sensor-guided ophthalmic surgical devices that can compensate physiological tremors during surgery.[3–4,6] With such systems, OCT-distal sensors should be disposable with a long sensing range. It has been shown that common-path (CP) swept-source OCT (SSOCT) allows the use of a disposable probe of an arbitrary length. It also can be made to be compact, simple, free from dispersion and polarization mismatches, and tolerable to system vibrations.

However, bare fiber probes, commonly used as a sensing probe for CP-OCT, have two main drawbacks: strong divergence of the sample beam and dependence of OCT sensitivity on the refractive index of the working environment. To overcome the strong divergence of bare fiber probes, various lensed probe systems have been proposed and demonstrated. These include fused coreless fiber,[9,10] ball lens,[11–14] GRIN lens,[15] and conical-frustum tip.[16] While most of them work well for standard OCT configurations, they do not work well for CP setups, especially in vitreous media (i.e., water). This is mainly caused by the inability to readily fabricate the reference surface with an optimized reflectivity. Those designed for CP-OCTs[10,12,15,16] used lens/air interfaces as the reference, and their performance could degrade significantly in water because the lens effectiveness and/or the reference power level are significantly reduced.

For this paper, we designed and fabricated elliptical high-refractive-index epoxy-lensed fiber probes that exhibit long working distances and large depths of focus (DOF) in vitreous media (i.e., water) compared to standard bare or half-ball-lensed fiber probes. The refractive index difference between the high-refractive-index epoxy and fiber core keeps the reference beam power independent of the working environment. Additionally, the availability of a wide range of epoxies with different indices allows fine-tuning of the reference reflectivity by mixing them in proportion. To validate our approach, we fabricated multiple probes with a range of beam expansion lengths and lens curvatures. We then measured the signal-to-noise ratio (SNR) of the lensed OCT probes as a function of the target depth and compared them with theoretically calculated SNR. The endoscopic OCT-distal sensors were then tested for OCT B-mode imaging using a phantom target comprising several layers of tape to confirm the improved performance of the proposed lensed fiber probes.

2 Design of Lensed Fiber Probe

A key performance metrics of OCT-distal sensors is long sensing depth, and the region of DOF outside the probe is considered the effective sensing range. The working distance, DOF, and beam waist depend on the beam expansion length and the lens curvature, which can be calculated with the *ABCD* matrix method.[17] For the lensed fiber, *ABCD* can be calculated as

*Address all correspondence to Soohyun Lee, E-mail: slee452@jhu.edu

†Present Address: GE Global Research Center, Niskayuna, New York, United States

$$\begin{bmatrix} A & B \\ C & D \end{bmatrix} = \begin{bmatrix} 1 & x \\ 0 & 1 \end{bmatrix} \begin{bmatrix} 1 & 0 \\ \frac{n_e - n_h}{n_e R} & \frac{n_h}{n_e} \end{bmatrix} \begin{bmatrix} 1 & L \\ 0 & 1 \end{bmatrix}, \quad (1)$$

where L is the length of expansion region, R is the surface radius of the lens, n_e and n_h are the refractive indices of the sample environment (i.e., in air or in water) and high-index epoxy, respectively, and x is the propagation distance from the lens surface. For the case of bare fiber probes, the second and third matrices are identity matrices, and x is the distance from the fiber end. Working distance can be calculated by finding x, satisfying $AC + a^2BD = 0$, where a is $\lambda/n_g\pi\omega_0^2$ for lensed fiber and $\lambda/\pi\omega_0^2$ for bare fiber. Beam waist diameter ($2\omega_f$) at the focal length is expressed as[18]

$$2\omega_f = 2\omega_0 \left[\left(\frac{n_g}{n_e} \right) \frac{A^2 + a^2B^2}{AD - BC} \right]^{\frac{1}{2}}, \quad (2)$$

where $2\omega_0$ is the mode-field diameter of the fiber and λ is the wavelength in vacuum. The DOF can be expressed as

$$\text{DOF} = \frac{2\pi n_e \omega_f^2}{\lambda}. \quad (3)$$

Figure 1 shows the calculated working distance, beam waist diameter, DOF, and effective sensing range as a function of beam expansion length and lens curvature. The working distance is a distance from lens surface to the beam waist, where a plus/minus sign indicates which side of the lens surface the beam waist lies. It is positive when the beam waist lies outside the probe, and, conversely, it is negative when the beam waist is virtual and occurs inside the fiber probe. To obtain effective sensing range longer than 500, 1000, 1500, or 2000 μm, beam expansion length must be longer than 157, 228, 282, and 327 μm, respectively. Lens curvature must be around 1/5 of the expansion length. Because the fiber has a 125-μm cladding, it is easier to make a lens of 60-μm curvature. Therefore, we set the lens curvature to 60 μm and targeted expansion region length around 300 μm, because it provides the longest effective sensing range (1.6 mm) for the curvature. The beam waist diameter of the targeted lensed fiber was expected to be 31 μm in water. The red stars indicate the geometry of fabricated lenses.

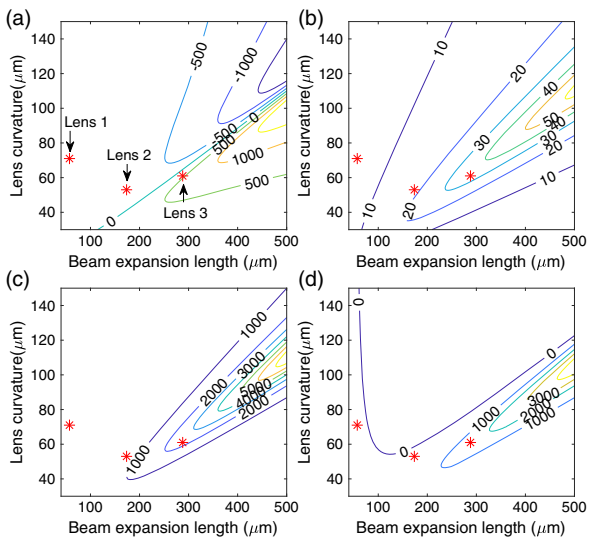

Fig. 1 Calculated (a) working distance, (b) beam waist diameter, (c) DOF, and (d) effective sensing range as a function of beam expansion length and lens curvature. Red stars indicate geometry of fabricated lenses.

3 Fabrication of Lensed Fiber and Lens Geometry

3.1 *Fabrication of Lensed Fiber*

The lensed fiber OCT sensor was fabricated using UV curable epoxy (Norland Optical Adhesive, $n = 1.7$). First, a semispherical lensed probe was fabricated by applying the epoxy to the fiber end, which naturally forms a semispherical shaped lens, owing to surface tension. Two fibers having semispherical epoxy ends were placed inline and brought together so that the epoxy lenses were in contact. We controlled axial and transverse positions of the fibers using x-y-z linear stages while monitoring them using digital microscopes and our CP-SSOCT system to ensure they were perfectly aligned. A beam expansion rod was fabricated by curing the combined epoxy using ultraviolet light and breaking connection with one of the fibers. The length of the expansion rod was controlled by changing the distance between fiber ends. The fabricated expansion rod length was limited to around 120 μm because of the limited amount of epoxy that could be applied to bare fibers. A beam expansion rod of ~240 μm was fabricated by applying more epoxy on the 120-μm expansion rod via repeating the process. The end of the expansion rod was capped by applying a semispherical epoxy lens. This process can be highly reproducible when the direction and position of the fiber are controlled precisely. Another factor in the reproducibility is the amount of the epoxy picked up by the fiber. This is also related to the precise control of the fiber. An epoxy lens can be quickly distorted when even a small amount of epoxy touches the sidewall of the fiber or the expansion rod. However, once epoxy forms a spherical shape at fiber end and expansion rod end, the shape of the lens is highly repeatable and durable. Figure 2 schematically shows the fabrication steps from bare fiber to the designed elliptical-lensed fiber. For comparison, we also constructed lensed fibers having different expansion region lengths and lens curvatures. Lens 1, lens 2, and lens 3 were fabricated by applying and curing spherical epoxy on bare fiber, 120-μm beam expansion rod, and 240-μm beam expansion rod, respectively.

3.2 *Lens Geometry*

Figure 3 shows *en-face* OCT images of the fabricated lensed fiber probe with lens 1, lens 2, lens 3, and a 240-μm

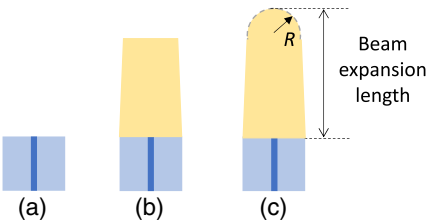

Fig. 2 Illustration of fabrication process: (a) preparing bare fiber, (b) constructing expansion rod, and (c) applying spherical surface on the expansion rod.

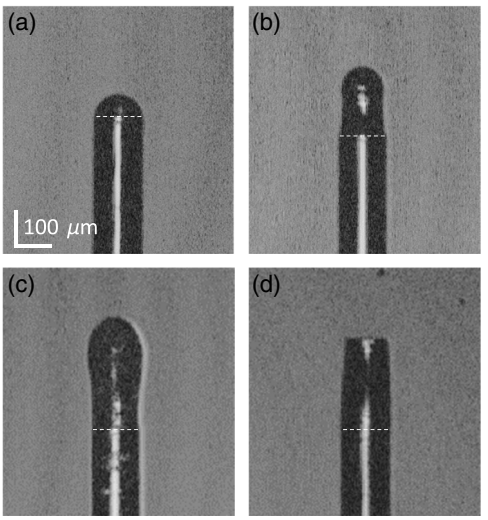

Fig. 3 *En-face* OCT images of fiber probe with (a) lens 1, (b) lens 2, (c) lens 3, and (d) 240-μm expansion rod. Dashed line shows interface between bare fiber and epoxy.

expansion rod. The curvature of the spherical surface was measured using OCT images with customized Matlab code, which uses least squares to fit a sphere on a manually selected edge. The length of beam expansion region was measured by our OCT system. Beam expansion lengths and curvatures of fabricated lenses are listed in Table 1. Lens 3 is the one closest to our design. Only lens 3 has positive working distance because it has a sufficient beam expansion area that allows the focusing of the beam. Lens 1 and lens 2 simply reduce beam divergence.

We measured and verified the output-beam characteristics of the fabricated probes by comparing the beam spot diameter measured from knife-edge method[19] to simulated beam diameter via the *ABCD* method. Figures 4(a) and 4(b) show the erf function result using the knife-edge measurement and resultant beam shapes of bare fiber and each lensed fiber at 1-mm distance. We performed knife-edge measurements of each lensed fiber at various distances. Figure 4(c) shows the measured and calculated beam diameter in air. The mode-field diameter was 3.2 μm, and the lens geometry listed in Table 1 was used for calculation. Calculated and measured beam diameters match reasonably well throughout the distance ranges, confirming the measured geometry of our lens and calculation. Although it is difficult to measure beam diameter in water, we can use the calculated values shown in Fig. 4(d).

Table 1 Fabricated lens geometry and theoretically calculated working distance, beam waist diameter, and effective sensing range.

	Lens length (μm)	Surface radius (μm)	Working distance (μm)	Beam waist diameter (μm)	Effective sensing range (μm)
Lens 1	57.2	71	−43	8	14
Lens 2	173.6	53	−240	18	80
Lens 3	288	61	476	33	1600

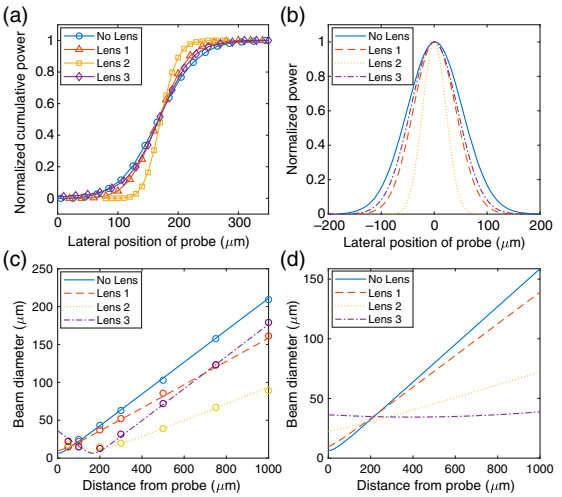

Fig. 4 (a) The erf function result using knife-edge measurement at 1 mm away from probe. (b) Beam shape from fitting the erf functions in (a). Measured (shapes) and calculated (lines) beam diameter of each lensed fiber in (c) air and (d) water, depending on distance from probe.

4 Performance of the Lensed Fiber Probes

4.1 *Signal-to-Noise Ratio*

The SNR versus depth was measured to show improved performance of the lensed fiber probes. Theoretical SNR was also calculated using the following equation to confirm the measured SNR:

$$\frac{S}{N} = \frac{2\frac{1}{L_{\text{Proc}}}\left(\frac{\eta q}{h\nu}\right)^2 P_r P_s}{\left[\left(\frac{\eta q}{h\nu}\right)^2 NEP^2 + 2\frac{\eta q^2}{h\nu}(P_r+P_s) + \left(\frac{\eta q}{h\nu}\right)^2 RIN(P_r+P_s)^2\right]\frac{2B}{N}}. \tag{4}$$

For the calculation, the detector quantum efficiency (η) was 0.9, noise equivalent power (NEP) was 5 pW/$\sqrt{\text{Hz}}$ at 1-mm depth, relative intensity noise was −130 dB/Hz, the bandwidth of the optical receiver (B) was 68.8 MHz, and the number of samples (N) was 1376. The digital processing loss was set to 1.8 dB for a Hann window.[20] Sample power at each depth was estimated by returned sample beam diameter at the fiber end because the peak intensity of a Gaussian beam is inversely proportional to the square of the beam diameter. Coupling loss was considered when P_r and P_s were calculated. For reflected sample beam diameters, *ABCD* can be calculated as

$$\begin{bmatrix} A & B \\ C & D \end{bmatrix} = \begin{bmatrix} 1 & L \\ 0 & 1 \end{bmatrix}\begin{bmatrix} 1 & 0 \\ -\frac{n_h - n_e}{n_h R} & \frac{n_e}{n_h} \end{bmatrix}\begin{bmatrix} 1 & x \\ 0 & 1 \end{bmatrix}\begin{bmatrix} 1 & x \\ 0 & 1 \end{bmatrix} \times \begin{bmatrix} 1 & 0 \\ \frac{n_e - n_h}{n_e R} & \frac{n_h}{n_e} \end{bmatrix}\begin{bmatrix} 1 & L \\ 0 & 1 \end{bmatrix}. \tag{5}$$

A mirror was used as a sample, and the power at the fiber end was set to 0.15 mW to avoid saturation. Noise was limited by detector noise because of the low power. Detector noise has frequency dependence.[20] Thus, we estimated NEP from the measurement of detector noise (i.e., A-scan

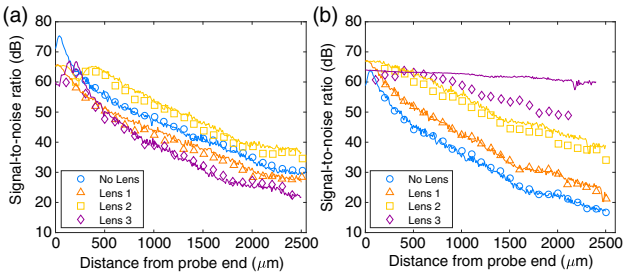

Fig. 5 Theoretically calculated (lines) and measured (shapes) SNR of each lensed fiber in (a) air and in (b) water.

image without an input signal) assuming NEP at 1 mm is 5 pW/$\sqrt{\text{Hz}}$.

Figures 5(a) and 5(b) show the SNR of each lensed fiber versus its depth in both air and water, respectively. Bare fiber showed relatively high SNR in air, despite its large divergence caused by higher reference power. However, it degraded significantly in water. Lens 3 showed the highest SNR in water. The 10-dB range of the bare fiber was 200 μm, and it increased to 1600 μm with lens 3. The measured and calculated SNR fits reasonably well throughout the distance range, except for lens 3 in water. The difference is probably caused by the large mode mismatching caused by the tight beam focus.

4.2 *Optical Coherence Tomography Imaging Performance*

To confirm the improved SNR and resolution, B-scan images of a phantom target comprising several layers of tape were obtained at various distances using the lensed fibers. The fiber probe was attached to a motorized translation stage (Thorlabs MT1-Z8), and the probe was scanned horizontally across the phantom. Figures 6 and 7 show the OCT images working in water and air, respectively. The OCT images showed similar trends as with the previous beam diameters and SNR measurements. In water, the designed lensed fiber

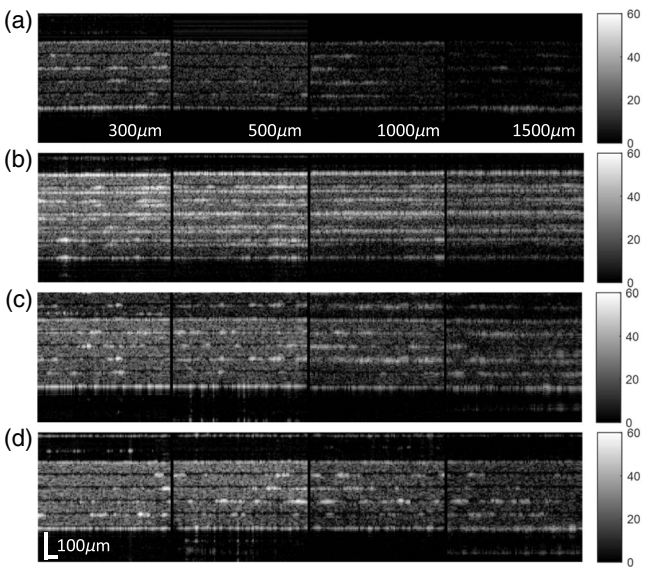

Fig. 6 B-mode OCT images of a phantom target made up of several layers of tapes obtained by fiber probe (a) without lens (bare fiber), (b) with lens 1, (c) with lens 2, and (d) with lens 3 in water.

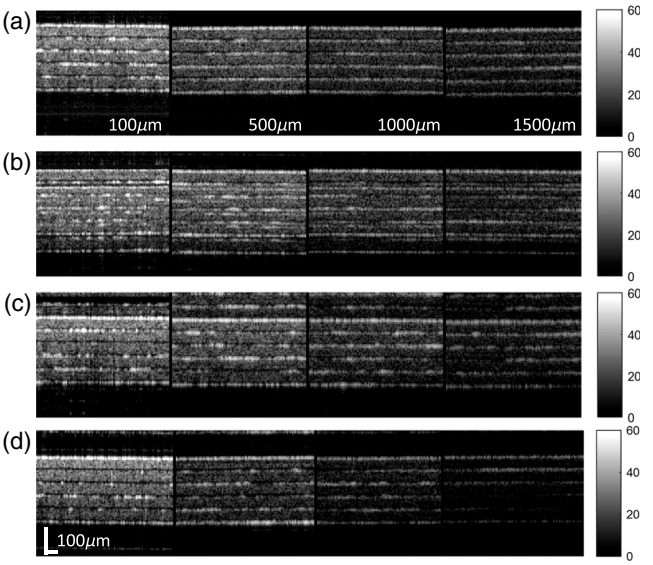

Fig. 7 B-mode OCT images of a phantom target made up of several layers of tapes obtained by fiber probe (a) without lens (bare fiber), (b) with lens 1, (c) with lens 2, and (d) with lens 3 in air.

showed the best image quality at all distances. All probes showed similar image quality at 300-μm distance except bare fiber, which has a lower SNR because of low reflection at the fiber end. However, the designed lensed fiber showed better quality than other lensed fibers when the probe was further away from the sample because of its long working distance and DOF. The quality improvement from the designed lensed fiber can be clearly seen at the 1500-μm distance. In air, fiber probes without a lens and with lens 2 showed better quality, as expected. A fiber probe with lens 3, optimized for working in wet environments, showed the worst image quality because of strong divergence and smaller reference than bare fiber.

5 Conclusion

We have demonstrated that CP-SSOCT imaging and sensing in water can be enhanced using a high refractive index elliptical epoxy-lensed fiber probe. We designed lensed fibers having long working distances and DOFs in water to obtain sufficiently long effective distal sensing ranges. Enhanced performance was confirmed by SNR and B-scan OCT images. The SNR of the proposed fiber probe, compared to a bare fiber at a distance of 1.5 mm, was increased by 25 dB and the resolution improved from 476 to 47 μm. We can conclude that the improved performance in water indicates that such high refractive index epoxy-lensed fibers can work effectively in ophthalmic and vascular applications.

Acknowledgments

This work was supported by the Korean WC300 R&D Project.

References

1. M. J. Gora et al., "Endoscopic optical coherence tomography: technologies and clinical applications [Invited]," *Biomed. Opt. Express* **8**, 2405–2444 (2017).
2. S. Han et al., "Handheld forward-imaging needle endoscope for ophthalmic optical coherence tomography inspection," *J. Biomed. Opt.* **13**(2), 020505 (2008).

3. J. U. Kang et al., "Endoscopic functional Fourier domain common-path optical coherence tomography for microsurgery," *IEEE J. Sel. Topics Quantum Electron.* **16**, 781 (2010).
4. C. Song et al., "Fiber-optic OCT sensor guided, 'SMART' micro-forceps for microsurgery," *Biomed. Opt. Express* **4**(7), 1045 (2013).
5. K. M. Joos and J.-H. Shen, "Miniature real-time intraoperative forward-imaging optical coherence tomography probe," *Biomed. Opt. Express* **4**(8), 1342 (2013).
6. G. W. Cheon et al., "Accurate real-time depth control for CP-SSOCT distal sensor based handheld microsurgery tools," *Biomed. Opt. Express* **6**(5), 1942 (2015).
7. T. Asami et al., "Development of a fiber-optic optical coherence tomography probe for intraocular use," *Invest. Ophthalmol. Visual Sci.* **57**(9), OCT568 (2016).
8. M. Mura et al., "Use of a new intra-ocular spectral domain optical coherence tomography in vitreoretinal surgery," *Acta Ophthalmol.* **94**, 246 (2016).
9. S. Y. Ryu et al., "Lensed fiber probes designed as an alternative to bulk probes in optical coherence tomography," *Appl. Opt.* **47**(10), 1510 (2008).
10. Y. Qiu et al., "Ultrathin lensed fiber-optic probe for optical coherence tomography," *Biomed. Opt. Express* **7**(6), 2154 (2016).
11. M. Zhao, Y. Huang, and J. U. Kang, "Sapphire ball lens-based fiber probe for common-path optical coherence tomography and its applications in corneal and retinal imaging," *Opt. Lett.* **37**(23), 4835 (2012).
12. K. Singh, D. Yamada, and G. Tearney, "Common path side viewing monolithic ball lens probe for optical coherence tomography," *Sovrem. Tehnol. Med.* **7**(1), 29 (2015).
13. S.-B. Wen et al., "Low-cost, high-precision micro-lensed optical fiber providing deep-micrometer to deep-nanometer-level light focusing," *Opt. Lett.* **41**(8), 1793 (2016).
14. M. Marrese et al., "70 μm diameter optical probe for common-path optical coherence tomography in air and liquids," *Opt. Lett.* **43**(24), 5929 (2018).
15. D. Wang et al., "Common-path optical coherence tomography using a microelectromechanical-system-based endoscopic probe," *Appl. Opt.* **55**(25), 6930 (2016).
16. J.-H. Kim, J.-H. Han, and J. Jeong, "Common-path optical coherence tomography using a conical-frustum-tip fiber probe," *IEEE J. Sel. Top. Quantum Electron.* **20**(2), 6800407 (2013).
17. H. Kogelnik, "On the propagation of Gaussian beams of light through lenslike media including those with a loss or gain variation," *Appl. Opt.* **4**(12), 1562 (1965).
18. W. L. Emkey and C. A. Jack, "Analysis and evaluation of graded-index fiber-lenses," *J. Lightwave Technol.* **5**, 1156 (1987).
19. J. A. Arnaud et al., "Technique for fast measurement of Gaussian laser beam parameters," *Appl. Opt.* **10**(12), 2775 (1971).
20. B. Johnson et al., "Swept light sources," Chapter 21 in *Optical Coherence Tomography*, W. Drexler and J. Fujimoto, Eds., pp. 639–658, Springer, Cham (2015).

Soohyun Lee is a PhD student in the Electrical and Computer Engineering Department, Johns Hopkins University. She received her BS and MS degrees in electrical engineering from Korea Advanced Institute of Science and Technology in 2010 and 2012, respectively. She worked as a research engineer at the Electronics and Telecommunications Research Institute from 2012 to 2016.

Changho Lee is currently an assistant professor at Chonnam National University (CNU), Republic of Korea, since 2017. He received his PhD from Kyungpook National University in 2013. Before joining the CNU, he worked as an assistant research professor and a postdoctoral fellow at Pohang University of Science and Technology from 2013 to 2016 and Johns Hopkins University from 2016 to 2017.

Ruben Verkade is a graduate student in mechanical engineering from Eindhoven University of Technology (TU/e). He received his BSc degree in mechanical engineering from TU/e in 2016. As part of his master's, he did his internship under Dr. Kang in the summer of 2018, where he researched optical coherence tomography for retinal detection. Currently, he is pursuing his graduation project at DEMCON Macawi Respiratory Systems.

Gyeong Woo Cheon received his BS degree in electrical engineering and his MS degree in biomedical engineering from Seoul National University in 2008 and in 2010, respectively. He worked at Korea Electrotechnology Research Institute as a researcher for two years and he received his PhD in electrical and computer engineering from Johns Hopkins University in 2016. Currently, he is a lead advanced computing engineer with General Electric Global Research.

Jin U. Kang is a Jacob Suter Jammer professor of electrical and computer engineering. He holds a joint appointment in the Department of Dermatology at the Johns Hopkins University School of Medicine and is a member of Johns Hopkins' Kavli Neuroscience Discovery Institute and Laboratory for Computational Sensing and Robotics. He is a fellow of the Optical Society of America, the International Optics Society, and the American Institute for Medical and Biological Engineering.